JACS
JOURNAL OF THE AMERICAN CHEMICAL SOCIETY
pubs.acs.org/JACS
Article

Enhanced Nanoconfinement of Copper-Organic Interfaces within Phthalocyanine Frameworks for Selective Electroreduction of CO to Acetate

Quanquan Yang,[#] Yaqi Chen,[#] Nengji Liu, Shengxu Li, Mengwei Chen, Wanzhen Zheng, Yubin Fu, Junyi Han,* Raul D. Rodriguez,* Yang Hou,* and Tao Zhang*

Cite This: J. Am. Chem. Soc. 2025, 147, 22132−22140
Read Online
ACCESS | Metrics & More | Article Recommendations | Supporting Information

ABSTRACT: Acetate is an essential raw material in the chemical industry, supporting sustainable processes and efficient carbon utilization, driving interest in electrochemical CO-to-acetate conversion. However, this process is limited by catalyst instability and the complexity of the reaction pathway, making precise control difficult. Herein, we engineer nanoconfined copper-organic interfaces within a series of nucleophilic substituted heterocyclic copper phthalocyanine covalent organic frameworks (CuPc-COFs) with AA' stacking configuration to selectively steer CO electroreduction toward acetate. This architecture stabilizes low-coordination Cu clusters—generated via partial reduction of phthalocyanine Cu sites—and fosters synergistic CuPc-Cu cluster interactions, creating an active interfacial microenvironment that enhances acetate selectivity. The optimized CuPc-COF achieves a Faradaic efficiency (FE) of 53.5% for acetate at −0.9 V vs RHE. Operando X-ray absorption spectroscopy (XAS) confirms the in situ formation of highly reactive copper-organic interfaces, while in situ FTIR spectroscopy and DFT calculations reveal that low-coordinated Cu clusters strengthen *CO bridge adsorption (*CO_B) and promote *COCO dimerization. Additionally, heterocyclic linkers provide electron donation, stabilizing the Cu clusters and improving the structural integrity. This work elucidates the critical role of nanoconfined interface engineering in C−C coupling and establishes a design paradigm for advanced CO electroreduction catalysts.

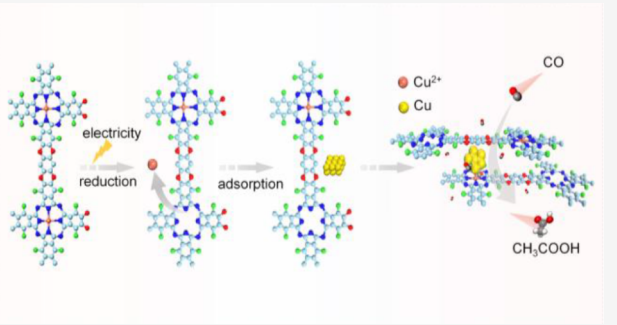

INTRODUCTION

Acetate is indispensable in the chemical industry, playing an essential role in advancing sustainable chemical processes and efficient carbon utilization.[1−3] The challenge is that its current industrial production heavily depends on fossil fuels, particularly through methanol carbonylation, contributing to significant carbon emissions and high energy consumption.[4−7] In contrast, renewable energy-driven electrochemical conversion methods[6−9] present an environmentally friendly, sustainable, and efficient solution for converting CO directly into acetate.[9−12] However, this process faces major challenges due to complex reaction pathways and challenges in achieving high selectivity for acetate in the electrochemical CO reduction reaction (eCORR).[6,13−15]

Covalent organic frameworks (COFs)[16−18] have emerged as promising candidates in electrochemical applications[19,20] due to their tunable pore structures[21] and rich active sites.[22,23] In eCORR, acetate generation typically depends on the synergy between copper (Cu) active sites,[24−26] facilitating key reaction steps such as C−C coupling and hydrogenation.[26−29] Although single-atom metal catalysts are commonly employed in COF-based studies,[30] the presence of multiple active sites in electrosynthesis reactions has significantly enhanced reaction selectivity and efficiency.[31−33] Recently, Cu-phthalocyanine (CuPc) has attracted considerable attention due to its unique electrocatalytic properties.[21,34−36] Studies indicate that CuPc can undergo partial in situ transformation into composite metal catalysts with nanocluster loadings, providing new avenues for optimizing catalytic performance.[37]

To further enhance catalytic performance, we designed and synthesized a series of CuPc-COFs with an AA' stacking configuration,[35,38] aiming to stabilize Cu active sites and improve acetate selectivity.[39] The distinctive structure of CuPc-COFs anchors the partially formed Cu clusters and facilitates synergy with the phthalocyanine Cu sites,[40,41] thus forming the Cu cluster-phthalocyanine Cu interfaces, a reaction microenvironment similar to the synergistic interaction of copper-organic (Cu-organic) interfaces. This Cu-

Received: April 20, 2025
Revised: June 4, 2025
Accepted: June 4, 2025
Published: June 11, 2025

https://doi.org/10.1021/jacs.5c06660
J. Am. Chem. Soc. 2025, 147, 22132−22140

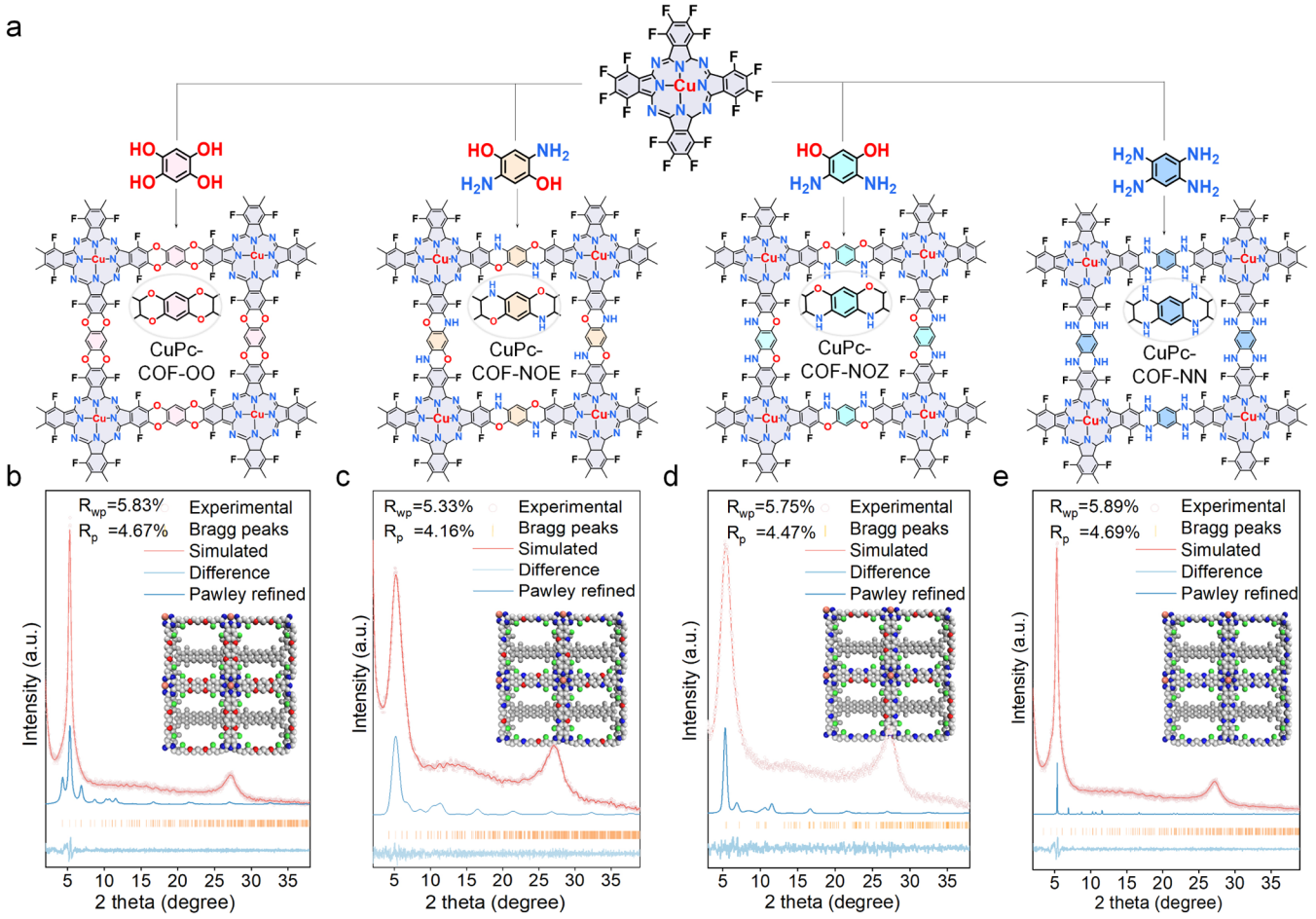

Figure 1. Schematic diagram of the synthesis of CuPc-COFs and crystal characterization. (a) Schematic diagram of the synthesis of CuPc-COFs; Experimental, simulated, and refined PXRD patterns and difference curve for (b) CuPc-COF-OO, (c) CuPc-COF-NOE, (d) CuPc-COF-NOZ, and (e) CuPc-COF-NN. The insets at the top show the structural model with AA' stacking (atomic color scheme: C = gray, N = blue, O = red, Cu = orange, F = green).

organic interface synergy significantly enhances the selectivity for C_{2+} products and acetate by optimizing the electronic structure, promoting charge separation, and improving the adsorption and conversion of reaction intermediates.[37,42] In the eCORR test, the CuPc-COFs catalysts can obtain a maximum acetate Faraday efficiency (FE) of about 53.5% at −0.9 V vs RHE. Detailed experimental analysis and theoretical calculations have allowed us to elucidate the mechanism underlying acetate generation, emphasizing the role of the Cu-organic interface within CuPc-COFs nanopores in promoting C−C coupling, and demonstrate that the bonding motifs in the CuPc-COFs exhibit electron-donating capabilities, which stabilize low-coordination Cu clusters, thereby enhancing their catalytic activity for eCORR.

RESULTS AND DISCUSSION

Synthesis Methodology. The synthesis of CuPc-COFs-OO was completed in 5 days with an 83% yield. The reaction involved the use of CuPc and benzene-1,2,4,5-tetraol monomers as structural units, employing a nucleophilic aromatic substitution reaction (SNAr) in a mixed solvent (DMAc/mesitylene (0.9/0.1 mL) and Et_3N (0.1 mL)) at 150 °C. Similarly, CuPc-COF-NOE, CuPc-COF-NOZ, and CuPc-COF-NN were also synthesized under identical conditions using 2,5-diaminobenzene-1,4-diol, 4,6-diaminobenzene-1,3-diol, and benzene-1,2,4,5-tetraamine as linkers, with yields of approximately 80% (Figure 1a).

Chemical structures. To characterize the structure and composition of CuPc-COFs, Fourier transform infrared (FTIR) spectroscopy was employed. Comparative analysis of the precursors and CuPc-COFs revealed key evidence of structural evolution: the broad −OH stretching vibrations (3200−3600 cm^{-1}) from the phenolic linkers and the sharp $-NH_2$ deformation bands (1596 cm^{-1}) from the amine-containing monomers were significantly reduced to near-vanishing in all COF spectra, confirming that these nucleophilic groups were consumed during the SNAr reaction. At the same time, new vibrational features appeared at 1280/1152 cm^{-1} (assigned to C−O symmetric/asymmetric stretching in the aromatic ether bond), which directly corresponds to the covalent bonds formed between the perfluorocopper phthalocyanine (CuPc) core and the respective linkers (Figure S1). Notably, the intensity of the retained C−F vibration at 950 cm^{-1} was reduced by 38% compared to that of the CuPc precursor, which is consistent with partial fluorine substitution while maintaining the structural integrity of the conjugated nodes, the phenomenon that has been well demonstrated in SNAr-based framework assembly.

Crystal structures. The crystal structure of CuPc-COFs was analyzed using a combination of PXRD analysis and computer

https://doi.org/10.1021/jacs.5c06660
J. Am. Chem. Soc. 2025, 147, 22132−22140

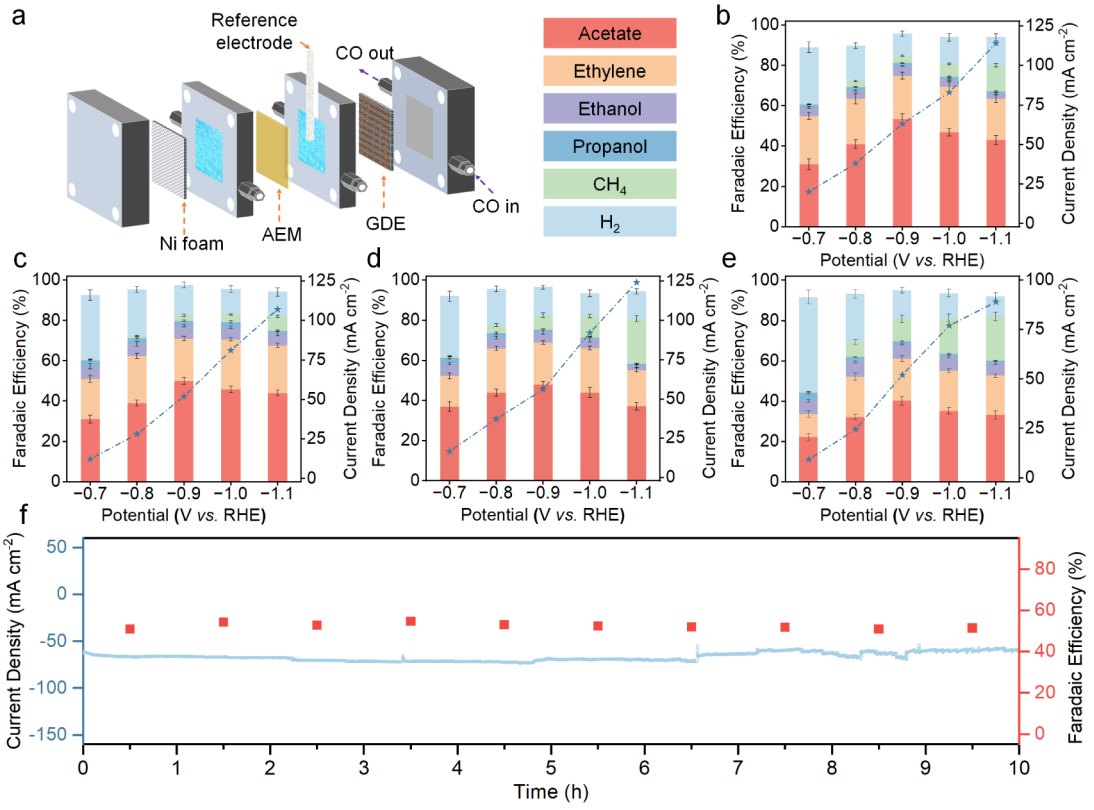

Figure 2. Electrochemical CORR performances. (a) Flow-cell device schematic diagram; Faradaic efficiency and the relationship between the potential and the applied current density for (b) CuPc-COF-OO, (c) CuPc-COF-NOE, (d) CuPc-COF-NOZ, and (e) CuPc-COF-NN; (f) Faradaic efficiency and current density vs time at 0.9 V vs RHE.

simulations. CuPc-COFs exhibit excellent crystallinity, as evidenced by a series of strong PXRD peaks around 5.6° and 27.3°, corresponding to the (110) and (001) planes, respectively. A series of PXRD peaks were obtained at lattice parameters (a = 20.5213°, b = 19.9969°, c = 3.36°) using the AMM2 (C2 V-14) cluster space for structural modeling (Table S1 and S2), consistent with the experimental data. As illustrated in the insets of Figure 1b–e, the AA' structure forms a staggered lattice with a distance value of a/2. In contrast, the AA stacking lattice cannot reproduce the observed PXRD pattern (Figure S2). As observed in the scanning electron microscopy (SEM) (Figure S3) and transmission electron microscopy (TEM) (Figures S4 and S5) images, CuPc-COFs exhibited a predominantly blocky morphology.

Furthermore, energy dispersive X-ray (EDX) imaging revealed that Cu(II) was homogeneously distributed throughout the COF matrix without any observable precipitation on the surface (Figure S6). Furthermore, the CuPc-COFs have excellent thermal and chemical stabilities (Figures S7 and S8).

Electrochemical CORR Performances. We first deposited CuPc-COF-X samples onto gas diffusion electrodes (GDEs) by spraying them with a carbon black and a Nafion binder mixture. We measured their CO reduction performance in a flow cell using 1.0 M KOH as the electrolyte (Figure 2a). Gas and liquid products were analyzed and quantified by using gas chromatography (GC) and proton nuclear magnetic resonance (^{1}H NMR). Figure 2a illustrates a schematic of the flow-cell eCORR setup. Figure 2b–e depicts the relationships between FE and the potential of the products as functions of the applied current density. Within the testing range of −0.7 to −1.1 V vs RHE, all CuPc-COF-X samples showed catalytic performance dominated by C_{2+} products, and the FE of acetate were above 40%, among which CuPc-COF-OO has the optimal acetate selectivity, reaching the FE of acetate was 53.5 ± 2.5% (Figure 2b–e). Additionally, GDEs prepared by carbon black (XC-72R) combined with catalysts alleviated the CO mass limitations,[43] allowing the CuPc-COF-OO partial current density for acetate achieved the between 33.7–49.0 mA cm^{-2} in the range of −0.9 to −1.1 V vs RHE. Furthermore, CuPc-COF-OO exhibits excellent stability at a voltage of −0.9 V vs RHE, and the FE of acetate does not change significantly (Figure 2f). Overall, CuPc-COF-X catalysts exhibited excellent activity, selectivity, and stability in CO electrolysis to produce acetate, significantly outperforming conventional Cu-based eCORR catalysts, which typically achieve only 30–40% FE.[44,45]

Structural Evolution of the Catalysts During eCORR. The generation rate of C_{2+} is typically constrained by the C–C coupling step that occurs between adjacent *CO(H) adsorption events, where the *COCO intermediate formation is widely hypothesized as the dominant pathway on conventional Cu surfaces under high *CO coverage conditions.[14,46] This step is highly sensitive to the surface structure of Cu and often involves the participation of more than two Cu sites, as evidenced by the cooperative stabilization of *COCO intermediates on adjacent Cu pairs.[47] Although previous reports have indicated that single-atom Cu sites may undergo C–C coupling via heterogeneous pathways (e.g., *CO + CO_2 → *$C_2O_3^-$), we hypothesize that the higher Gibbs free energy ($\Delta G \approx 1.8$ eV) compared to multisite coupling ($\Delta G \approx 0.9$ eV) may impede this process due to insufficient orbital overlap and

https://doi.org/10.1021/jacs.5c06660
J. Am. Chem. Soc. 2025, 147, 22132–22140

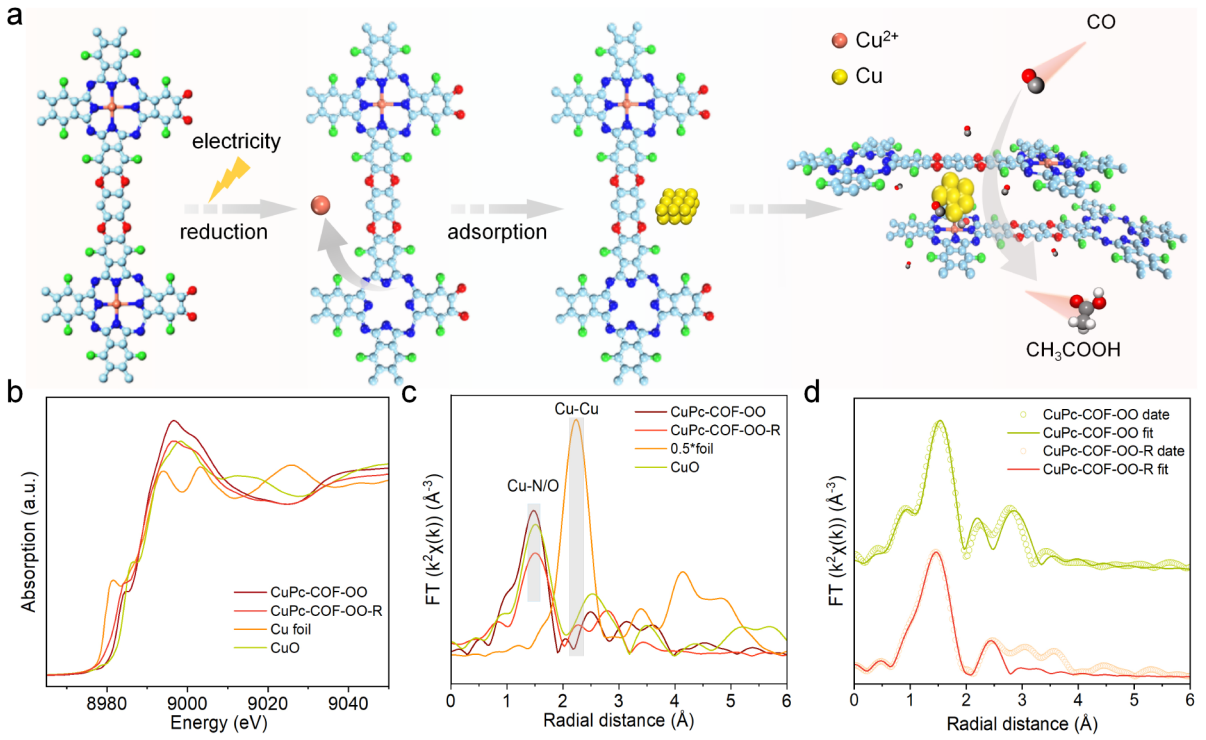

Figure 3. Structural evolution of the catalysts during the CORR. (a) Schematic diagram of the structural evolution of the catalyst during the CORR process; (b) comparison of Cu K-edge XANES spectra for the CuPc-COF-OO and CuPc-COF-OO-R; (c) comparison of Cu K-edge EXAFS, shown in k^2 weighted *R*-space for the CuPc-COF-OO and CuPc-COF-OO-R; (d) Cu K-edge EXAFS (points) and fit (line) for the CuPc-COF-OO and CuPc-COF-OO-R.

asymmetric adsorption configurations.[48,49] For CuPc-COF-X, its excellent C_{2+} activity leads us to hypothesize that there may be two adjacent Cu active sites or Cu clusters in the structure.

Consequently, X-ray absorption near-edge structure (XANES) spectroscopy was employed to examine the local coordination environment of CuPc-COF-OO both before and after the reaction (Figure 3). To visually observe the structural evolution of CuPc-COF-OO during the eCORR process, it was demonstrated by extended X-ray absorption fine structure (EXAFS) spectrum and fitting structure at constant potential −0.9 V vs RHE that the phthalocyanine Cu center in CuPc-COF would partially reduce with the application of potential, manifested as the emergence of Cu clusters (Figure 3b,c). The Cu−N bond distance in CuPc-COF-OO and CuPc-COF-OO-R (The "R" designation indicates the reduced state of the COF framework after electrochemical activation, characterized by partial $Cu^{2+} \rightarrow Cu^{+}/Cu^{0}$ reduction) remains almost unchanged (Table S3), while the corresponding coordination number is reduced from 4.1 to 3.0. This suggests that the Cu(II) coordination center of the main framework may undergo reduction to low-valent Cu^{0}/Cu(I) with a smaller coordination number.

Furthermore, high-resolution transmission electron microscopy (HRTEM) images demonstrate that the ultrafine particles in CuPc-COF-OO-R are uniformly dispersed with a lattice spacing of 0.2 nm, corresponding to the (111) plane of the Cu nanoparticles (Figure S9). In addition, we further characterized the surface structure and composition of CuPc-COF-OO-R by quasi-in situ X-ray photoelectron spectroscopy (XPS) measurements (Figure S10), and the surface structure is stable after reaction (Figure S11). We successfully obtained the change of the Cu valence state after CO electrolysis. The Cu 2p XPS spectrum (Figure S10c) shows that the Cu^{2+} in the CuPc molecule is partially reduced to metallic Cu during the reaction, which is consistent with the results of XAS and HRTEM analysis (Figures S12 and S9). At the same time, the O−Cu peak (531.4 eV) appeared in the O 1s XPS spectrum of CuPc-COF-OO-R (Figure S10b), and the N−Cu peak can still be observed in the N 1s XPS spectrum after the eCORR (Figure S10d). Combined with the above characteristics, it can be clearly confirmed that the Cu phthalocyanine ions in CuPc-COF-OO have been partially converted into low-coordination Cu clusters modified by organic ligands in situ, forming a Cu-organic interface. The XPS spectrum of CuPc-COF-NN-R also proves the generation of a Cu-organic interface (Figure S13). This is attributed to the distinctive AA' spatial configuration of phthalocyanine Cu in CuPc-COF-OO, which serves to self-limit the growth of nanoparticles. Furthermore, DFT calculations show that the Cu low-coordination clusters are strongly anchored at the interlayer connection sites (adsorption energy of −0.18 eV) and the phthalocyanine centers are weakly bound (Figure S14), while the rigid crystal framework forces the interlayer distance to be fixed, spatially confining the clusters to subnanometer sizes (XAFS Cu−Cu CN = 0.9 ± 0.5) (Table S3).

To further elucidate the essential role of the Cu-organic interface in facilitating C_{2+} product formation, we designed and synthesized three distinct catalytic systems: (i) commercial nanoscale Cu particles, (ii) a physical mixture of Cu particles and CuPc (CuPc-Cu), and (iii) a single-layer graphene oxide nanoplatelet-supported CuPc composite that mimics the layered COF structure (CuPc-GO) (Figures S15 and S16). The results demonstrate that the CuPc-Cu hybrid exhibits superior C_{2+} production compared to commercial pristine Cu

https://doi.org/10.1021/jacs.5c06660
J. Am. Chem. Soc. 2025, 147, 22132−22140

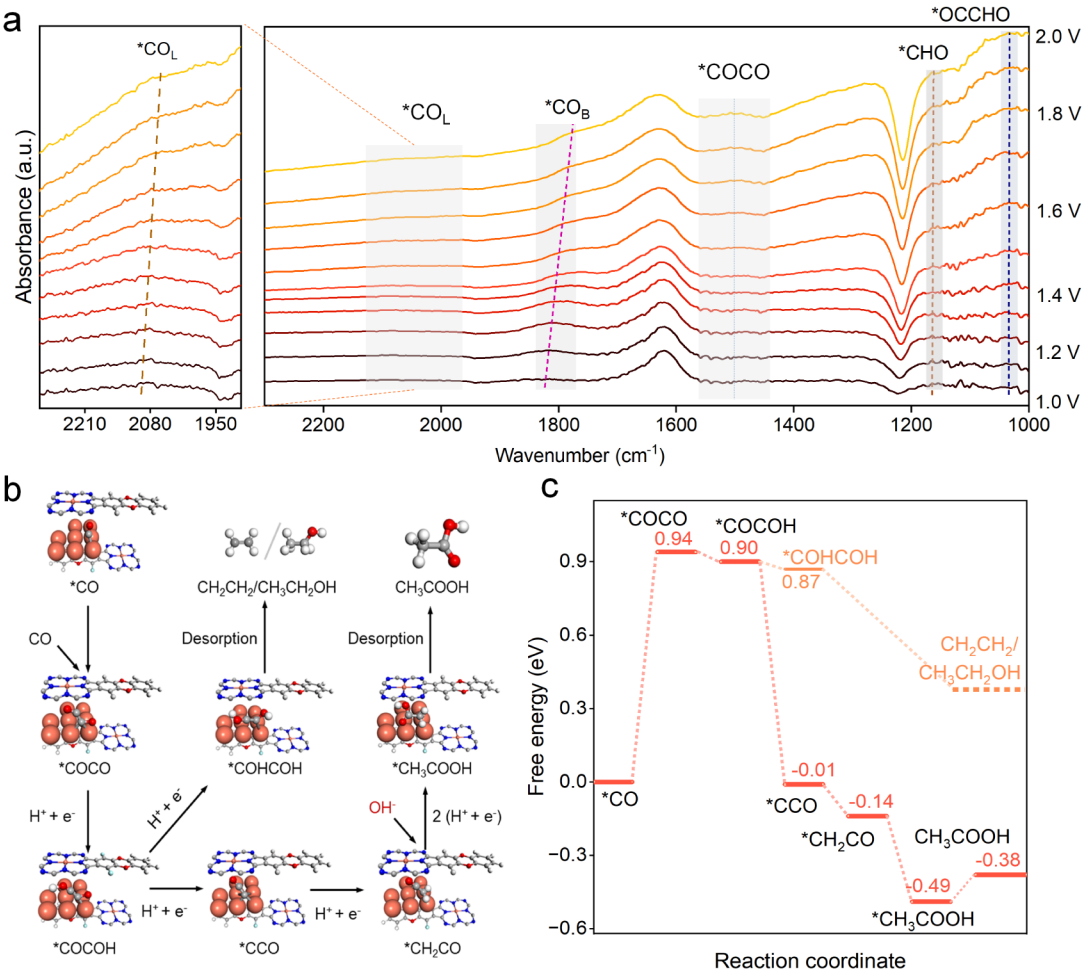

Figure 4. Mechanism exploration characterization. (a) In-situ FTIR spectroscopy under the potential from −1.0 to −2.0 V; (b) catalytic mechanism of CuPc-COF-OO to acetate via CORR; (c) calculated Gibbs free energy diagrams for CORR on the CuPc-COF-OO.

nanoparticles, however, the relatively large size of Cu nanoparticles limits the formation of a well-defined Cu-organic interface, resulting in only marginal catalytic enhancement (Figure S17). In contrast, the CuPc-GO system, where CuPc alone participates in the reaction, yields only trace amounts of methane and negligible C_{2+} products, indicating a lack of sufficient active sites for efficient C−C coupling. These pronounced differences underscore the critical synergistic effect between the stabilized low-coordination Cu clusters and the CuPc-derived organic interface, which collectively promote CO activation and selective C−C bond formation. In summary, the existence of Cu-organic interface is the key to the strong electrocatalytic activity and high selectivity in the preparation of acetate of CuPc-COF.

Mechanism Exploration. To identify the key intermediates involved in the formation of acetate during the eCORR process, we employed in situ FTIR spectroscopy using CuPc-COF-OO as the catalyst, with a scanning potential range of −1.0 to −2.0 V. The experimental results demonstrate that the vibrational signal intensity of bridge-adsorbed CO ($*CO_B$, 1820 cm^{-1}) is significantly higher than that of linearly adsorbed CO ($*CO_L$, 2082 cm^{-1}) (Figure 4a). This observation suggests the dominant role of the bridge configuration during the reaction, primarily attributed to the synergistic stabilization effect of dual-metal sites.[50] Further analysis combining synchrotron radiation XAS and density functional theory (DFT) calculations reveals that Cu−Cu atomic pairs (2.56 Å) in low-coordination Cu clusters establish a C−O−Cu_2 three-center bonding configuration (Table S3), which substantially reduces the activation free energy barrier (ΔG) for the critical C−C coupling step from 1.23 to 0.94 eV (Figures 4c and S18 and S19).[6] Importantly, while the geometric and electronic synergy of Cu−Cu bonds serves as the primary driving force for C−C coupling, the hydrogen-bonding network within the Cu−N_4 coordination environment at the Cu-organic interface extends the surface residence time of *CHO (1180 cm^{-1}) intermediates through spatial confinement effects.[3] In addition, the *CO(H) mediates asymmetric C−C coupling, and the *COCO (1560 cm^{-1}) as a critical intermediate for C_{2+} formation in eCORR (Figures 4a and S20-22).[3] This synergistic interaction between the primary and secondary active sites formed by the Cu-organic interface not only optimized the selectivity of the C−C coupling pathway but also effectively suppressed the competing side reactions (e.g., ethylene or ethanol formation) caused by the competition of multiple active sites in conventional Cu-based catalysts.[50]

In light of the insights gained from the operando in situ FTIR results, we employed DFT calculations to investigate the energy profile of eCORR to acetate on CuPc-COF-OO. As has been demonstrated in previous studies,[51−53] we believe that C_{2+} generation often requires more than two Cu sites.

https://doi.org/10.1021/jacs.5c06660
J. Am. Chem. Soc. 2025, 147, 22132−22140

Meanwhile, according to the above characterization results, the Cu-organic interface formed by phthalocyanine Cu and Cu clusters or Cu ions may have a synergistic effect in promoting the formation of C_{2+} products, especially the formation of acetate. Although the precise structure of this hybrid complex is challenging to ascertain with certainty, a reconstructed CuPc-COF-OO-R structural model has been formulated based on experimental evidence. We propose a model based on a Cu cluster adjacent to the partially reduced CuPc-COF-OO-R structural fragment. This creates a closed space between the aggregated Cu clusters and the Cu ion centers of the upper and lower unreduced phthalocyanine units (Figure 4b). The subsequent DFT study will be based on this model, as illustrated in Figure 4c for the Gibbs free energy calculation results.

The low-coordinated Cu clusters on the Cu-COF surface enhance *CO adsorption via an upshifted d-band center, resulting in high surface *CO coverage that sterically hinders *H adsorption, thereby suppressing HER and favoring selective C_{2+} product formation (Figures S18 and S19).[54,55] The results in Figures 4b,c show that all active sites from the Cu−organic interface fell in the eCORR dominant zone. The calculated selectivity of the model is in agreement with the experimental observation of stable C_{2+} and acetate production with suppressed H_2 on CuPc-COFs. The reaction pathways are summarized in Figure 4b, with a more detailed thermodynamic profile regarding all reaction intermediates provided. For the C_{2+} pathways, CO adsorption followed by immediate *CO coupling shows the maximum uphill free energy change (ΔG). This is the potential-determining step (PDS) with a limiting potential ($U_{limiting}$) of −0.94 V. The subsequent reduction of *COCOH on the Cu-organic interface proceeds in major pathways (Figure 4c), including the CH_3COOH pathway via the formation of *CCO. The conversion from *COCOH to *CCO is thermodynamically more favorable (ΔG = −0.01 eV) than the alternative pathway to *COHCOH (ΔG = 0.87 eV), enabling eCORR to preferentially proceed toward CH_3COOH formation via the $*CH_2CO$ intermediate on CuPc-COF/Cu. The reason for the unfavored formation of *COHCOH lies in the fact that the protonation on O is accompanied by the cleavage of the previously formed the O−Cu bond. Our calculations demonstrate that highly undercoordinated Cu clusters at the Cu-organic interface inhibit competitive HER by enhancing *CO adsorption, thereby promoting C−C coupling to form *CCO. Furthermore, the confined space between the Cu cluster and adjacent single Cu center affords an extra O−Cu bond to stabilize the *COCOH intermediate by breaking the linear scaling relation with *CO. Next, eCORR proceeds preferentially toward CH_3COOH formation through $*CH_2CO$. In summary, the synergistic interaction between low-coordination Cu clusters and Cu phthalocyanine molecules at the Cu-organic interface ultimately enables the high selectivity and catalytic efficiency for acetate production, establishing a new paradigm for the rational design of multiactive-site cooperative catalytic systems.

CONCLUSION

Here, we successfully synthesized Cu phthalocyanine-based covalent organic frameworks (CuPc-COFs) with a distinctive AA' stacking architecture. This unique structure facilitates the formation of Cu-organic interfaces within the COF nanopores during eCORR, which simultaneously enhances active site exposure, reduces electron transfer resistance, and stabilizes low-coordination Cu clusters for *CO bridge adsorption ($*CO_B$) intermediates. These synergistic effects significantly promote the electrochemical synthesis of the critical *COCO intermediate. The optimized Cu-organic interface markedly strengthens C−C coupling, endowing the catalyst with exceptional performance in the electrochemical CO-to-acetate conversion, achieving a remarkable FE of 53.5%, while providing a highly selective and stable pathway for acetate formation. These findings demonstrate the tremendous potential of Cu-COFs for enhancing the CO electroreduction efficiency and offer valuable insights for future research directions, including the functionalization of organic linkers and the incorporation of alternative metal centers to further engineer the catalytic properties of these COF materials.

ASSOCIATED CONTENT

Supporting Information

The Supporting Information is available free of charge at https://pubs.acs.org/doi/10.1021/jacs.5c06660.

Additional experimental details, materials and methods, data analysis of FT-IR spectra, Raman spectra, XPS spectra, crystalline domain size distribution, including supplementary SEM and TEM images, etc.PDF)

AUTHOR INFORMATION

Corresponding Authors

Tao Zhang − *Key Laboratory of Advanced Marine Materials, Ningbo Institute of Materials Technology and Engineering, Chinese Academy of Sciences, Ningbo 315201, China;* orcid.org/0000-0003-3218-0571; Email: tzhang@nimte.ac.cn

Yang Hou − *Key Laboratory of Biomass Chemical Engineering of Ministry of Education, College of Chemical and Biological Engineering, Zhejiang University, Hangzhou 310027, China;* orcid.org/0000-0001-9795-8503; Email: yhou@zju.edu.cn

Raul D. Rodriguez − *Research School of Chemistry and Applied Biomedical Sciences, Tomsk Polytechnic University, Tomsk 634050, Russia;* orcid.org/0000-0003-4016-1469; Email: raul@tpu.ru

Junyi Han − *Key Laboratory of Advanced Marine Materials, Ningbo Institute of Materials Technology and Engineering, Chinese Academy of Sciences, Ningbo 315201, China;* Email: hanjunyi@chem.eng.osaka-u.ac.jp

Authors

Quanquan Yang − *Key Laboratory of Advanced Marine Materials, Ningbo Institute of Materials Technology and Engineering, Chinese Academy of Sciences, Ningbo 315201, China; School of Materials Science and Engineering, Zhejiang Sci-Tech University, Hangzhou 310018, China;* orcid.org/0009-0007-7325-4991

Yaqi Chen − *Key Laboratory of Biomass Chemical Engineering of Ministry of Education, College of Chemical and Biological Engineering, Zhejiang University, Hangzhou 310027, China*

Nengji Liu − *Key Laboratory of Biomass Chemical Engineering of Ministry of Education, College of Chemical and Biological Engineering, Zhejiang University, Hangzhou 310027, China*

Shengxu Li − *Key Laboratory of Advanced Marine Materials, Ningbo Institute of Materials Technology and Engineering,*

Chinese Academy of Sciences, Ningbo 315201, China; orcid.org/0000-0003-1006-0237

Mengwei Chen − *Key Laboratory of Advanced Marine Materials, Ningbo Institute of Materials Technology and Engineering, Chinese Academy of Sciences, Ningbo 315201, China*

Wanzhen Zheng − *Key Laboratory of Advanced Marine Materials, Ningbo Institute of Materials Technology and Engineering, Chinese Academy of Sciences, Ningbo 315201, China; Key Laboratory of Biomass Chemical Engineering of Ministry of Education, College of Chemical and Biological Engineering, Zhejiang University, Hangzhou 310027, China*

Yubin Fu − *Center for Advancing Electronics Dresden (cfaed) & Faculty of Chemistry and Food Chemistry, Technische Universität Dresden, Dresden 01062, Germany;* orcid.org/0000-0002-2613-394X

Complete contact information is available at: https://pubs.acs.org/10.1021/jacs.5c06660

Author Contributions

#Q.Y. and Y.C. contributed equally to this work.

Notes

The authors declare no competing financial interest.

■ ACKNOWLEDGMENTS

T. Zhang acknowledges the National Natural Science Fund for Excellent Young Scholars (52322316), Distinguished Youth Foundation of Zhejiang Provincial Natural Science Foundation of China (LRG25E030001), International Cooperation and Exchanges Programme of Ningbo, Grant No. 2024H024 and the Key Research and Development Program of Ningbo (2022ZDYF020023). Y. Hou acknowledges the development project of Zhejiang Province's "Jianbing" and "Lingyan" (2023C01226), the National Natural Science Foundation of China (22425805, U22A20432, 22278364, 22211530045, 22238008, 22178308), the National Key Research and Development Program of China (2022YFB4002100), the Fundamental Research Funds for the Central Universities (226-2024-00060).

■ REFERENCES

(1) Liu, Y.; Chen, S.; Quan, X.; Yu, H. Efficient Electrochemical Reduction of Carbon Dioxide to Acetate on Nitrogen-Doped Nanodiamond. *J. Am. Chem. Soc.* **2015**, *137* (36), 11631−11636.

(2) Nie, S.; Wu, L.; Liu, Q.; Wang, X. Entropy-Derived Synthesis of the CuPd Sub-1nm Alloy for CO_2-to-Acetate Electroreduction. *J. Am. Chem. Soc.* **2024**, *146* (43), 29364−29372.

(3) Ding, J.; Li, F.; Ren, X.; Liu, Y.; Li, Y.; Shen, Z.; Wang, T.; Wang, W.; Wang, Y.-G.; Cui, Y.; et al. Molecular Tuning Boosts Asymmetric C−C Coupling for CO Conversion to Acetate. *Nat. Commun.* **2024**, *15* (1), 3641.

(4) Jin, J.; Wicks, J.; Min, Q.; Li, J.; Hu, Y.; Ma, J.; Wang, Y.; Jiang, Z.; Xu, Y.; Lu, R.; Si, G.; Papangelakis, P.; Shakouri, M.; Xiao, Q.; Ou, P.; Wang, X.; Chen, Z.; Zhang, W.; Yu, K.; Song, J.; Jiang, X.; Qiu, P.; Lou, Y.; Wu, D.; Mao, Y.; Ozden, A.; Wang, C.; Xia, B. Y.; Hu, X.; Dravid, V. P.; Yiu, Y.-M.; Sham, T.-K.; Wang, Z.; Sinton, D.; Mai, L.; Sargent, E. H.; Pang, Y. Constrained C_2 Adsorbate Orientation Enables CO-to-Acetate Electroreduction. *Nature* **2023**, *617* (7962), 724−729.

(5) Wang, X.; Chen, Y.; Li, F.; Miao, R. K.; Huang, J. E.; Zhao, Z.; Li, X.-Y.; Dorakhan, R.; Chu, S.; Wu, J.; et al. Site-Selective Protonation Enables Efficient Carbon Monoxide Electroreduction to Acetate. *Nat. Commun.* **2024**, *15* (1), 616.

(6) Ji, Y.; Chen, Z.; Wei, R.; Yang, C.; Wang, Y.; Xu, J.; Zhang, H.; Guan, A.; Chen, J.; Sham, T.-K.; Luo, J.; Yang, Y.; Xu, X.; Zheng, G. Selective CO-to-Acetate Electroreduction via Intermediate Adsorption Tuning on Ordered Cu−Pd Sites. *Nat. Catal.* **2022**, *5* (4), 251−258.

(7) Zhu, H.-L.; Huang, J.-R.; Zhang, M.-D.; Yu, C.; Liao, P.-Q.; Chen, X.-M. Continuously Producing Highly Concentrated and Pure Acetic Acid Aqueous Solution via Direct Electroreduction of CO_2. *J. Am. Chem. Soc.* **2024**, *146* (1), 1144−1152.

(8) Li, C. W.; Ciston, J.; Kanan, M. W. Electroreduction of Carbon Monoxide to Liquid Fuel on Oxide-Derived Nanocrystalline Copper. *Nature* **2014**, *508* (7497), 504−507.

(9) Li, J.; Kuang, Y.; Zhang, X.; Hung, W.-H.; Chiang, C.-Y.; Zhu, G.; Chen, G.; Wang, F.; Liang, P.; Dai, H. Electrochemical Acetate Production from High-Pressure Gaseous and Liquid CO_2. *Nat. Catal.* **2023**, *6* (12), 1151−1163.

(10) Xu, A.; Hung, S.-F.; Cao, A.; Wang, Z.; Karmodak, N.; Huang, J. E.; Yan, Y.; Sedighian Rasouli, A.; Ozden, A.; Wu, F.-Y.; Lin, Z.-Y.; Tsai, H.-J.; Lee, T.-J.; Li, F.; Luo, M.; Wang, Y.; Wang, X.; Abed, J.; Wang, Z.; Nam, D.-H.; Li, Y. C.; Ip, A. H.; Sinton, D.; Dong, C.; Sargent, E. H. Copper/Alkaline Earth Metal Oxide Interfaces for Electrochemical CO_2-to-Alcohol Conversion by Selective Hydrogenation. *Nat. Catal.* **2022**, *5* (12), 1081−1088.

(11) Shen, H.; Wang, Y.; Chakraborty, T.; Zhou, G.; Wang, C.; Fu, X.; Wang, Y.; Zhang, J.; Li, C.; Xu, F.; Cao, L.; Mueller, T.; Wang, C. Asymmetrical C−C Coupling for Electroreduction of CO on Bimetallic Cu−Pd Catalysts. *ACS Catal.* **2022**, *12* (9), 5275−5283.

(12) Joby, P.; Manojkumar, Y.; Rajendran, A.; Solomon, R. V. Computational Catalysis on the Conversion of CO_2 to Methane—an Update. *Front. Chem. Sci. Eng.* **2024**, *18* (11), 132.

(13) Overa, S.; Crandall, B. S.; Shrimant, B.; Tian, D.; Ko, B. H.; Shin, H.; Bae, C.; Jiao, F. Enhancing Acetate Selectivity by Coupling Anodic Oxidation to Carbon Monoxide Electroreduction. *Nat. Catal.* **2022**, *5* (8), 738−745.

(14) Li, H.; Jiang, Y.; Li, X.; Davey, K.; Zheng, Y.; Jiao, Y.; Qiao, S.-Z. C_{2+} Selectivity for CO_2 Electroreduction on Oxidized Cu-Based Catalysts. *J. Am. Chem. Soc.* **2023**, *145* (26), 14335−14344.

(15) Zhao, Y.; Wang, X.; Sang, X.; Zheng, S.; Yang, B.; Lei, L.; Hou, Y.; Li, Z. Spin Polarization Strategy to Deploy Proton Resource over Atomic-Level Metal Sites for Highly Selective CO_2 Electrolysis. *Front. Chem. Sci. Eng.* **2022**, *16* (12), 1772−1781.

(16) Ranallo, S.; Amodio, A.; Idili, A.; Porchetta, A.; Ricci, F. Electronic Control of DNA-Based Nanoswitches and Nanodevices. *Chem. Sci.* **2016**, *7* (1), 66−71.

(17) Fu, G.; Yang, D.; Xu, S.; Li, S.; Zhao, Y.; Yang, H.; Wu, D.; Petkov, P. S.; Lan, Z.-A.; Wang, X.; Zhang, T. Construction of Thiadiazole-Bridged sp^2 -Carbon-Conjugated Covalent Organic Frameworks with Diminished Excitation Binding Energy Toward Superior Photocatalysis. *J. Am. Chem. Soc.* **2024**, *146* (2), 1318−1325.

(18) Li, S.; Ma, R.; Xu, S.; Zheng, T.; Fu, G.; Wu, Y.; Liao, Z.; Kuang, Y.; Hou, Y.; Wang, D.; Petkov, P. S.; Simeonova, K.; Feng, X.; Wu, L.-Z.; Li, X.-B.; Zhang, T. Direct Construction of Isomeric Benzobisoxazole−Vinylene-Linked Covalent Organic Frameworks with Distinct Photocatalytic Properties. *J. Am. Chem. Soc.* **2022**, *144* (30), 13953−13960.

(19) Lin, S.; Diercks, C. S.; Zhang, Y.-B.; Kornienko, N.; Nichols, E. M.; Zhao, Y.; Paris, A. R.; Kim, D.; Yang, P.; Yaghi, O. M.; Chang, C. J. Covalent Organic Frameworks Comprising Cobalt Porphyrins for Catalytic CO_2 Reduction in Water. *Science* **2015**, *349* (6253), 1208−1213.

(20) Liu, H.; Chu, J.; Yin, Z.; Cai, X.; Zhuang, L.; Deng, H. Covalent Organic Frameworks Linked by Amine Bonding for Concerted Electrochemical Reduction of CO_2. *Chem* **2018**, *4* (7), 1696−1709.

(21) Zhi, Q.; Jiang, R.; Yang, X.; Jin, Y.; Qi, D.; Wang, K.; Liu, Y.; Jiang, J. Dithiine-Linked Metalphthalocyanine Framework with Undulated Layers for Highly Efficient and Stable H_2O_2 Electroproduction. *Nat. Commun.* **2024**, *15* (1), 678.

(22) Mei, Z.-Y.; Zhao, G.; Xia, C.; Cai, S.; Jing, Q.; Sheng, X.; Wang, H.; Zou, X.; Wang, L.; Guo, H.; et al. Regulated High-Spin State and

Constrained Charge Behavior of Active Cobalt Sites in Covalent Organic Frameworks for Promoting Electrocatalytic Oxygen Reduction. *Angew. Chem., Int. Ed.* **2023**, *62* (27), No. e202303871.
(23) Zhang, R.-Q.; Ma, A.; Liang, X.; Zhao, L.-M.; Zhao, H.; Yuan, Z.-Y. Cobalt Nanoparticle Decorated N-Doped Carbons Derived from a Cobalt Covalent Organic Framework for Oxygen Electrochemistry. *Front. Chem. Sci. Eng.* **2021**, *15* (6), 1550−1560.
(24) Lee, S. Y.; Jung, H.; Kim, N.-K.; Oh, H.-S.; Min, B. K.; Hwang, Y. J. Mixed Copper States in Anodized Cu Electrocatalyst for Stable and Selective Ethylene Production from CO_2 Reduction. *J. Am. Chem. Soc.* **2018**, *140* (28), 8681−8689.
(25) Zhang, Z.-Y.; Tian, H.; Jiao, H.; Wang, X.; Bian, L.; Liu, Y.; Khaorapapong, N.; Yamauchi, Y.; Wang, Z.-L. SiO_2 Assisted Cu^0 − Cu^+ − NH_2 Composite Interfaces for Efficient CO_2 Electroreduction to C_{2+} Products. *J. Mater. Chem. A* **2024**, *12* (2), 1218−1232.
(26) Zheng, Q.; Xu, H.; Yao, Y.; Dai, J.; Wang, J.; Hou, W.; Zhao, L.; Zou, X.; Zhan, G.; Wang, R.; et al. Cobalt Single-Atom Reverse Hydrogen Spillover for Efficient Electrochemical Water Dissociation and Dechlorination. *Angew. Chem., Int. Ed.* **2024**, *63* (19), No. e202401386.
(27) Zhao, Z.-H.; Huang, J.-R.; Liao, P.-Q.; Chen, X.-M. Highly Efficient Electroreduction of CO_2 to Ethanol via Asymmetric C−C Coupling by a Metal−Organic Framework with Heterodimetal Dual Sites. *J. Am. Chem. Soc.* **2023**, *145* (49), 26783−26790.
(28) Yang, B.; Chen, L.; Xue, S.; Sun, H.; Feng, K.; Chen, Y.; Zhang, X.; Xiao, L.; Qin, Y.; Zhong, J.; et al. Electrocatalytic CO_2 Reduction to Alcohols by Modulating the Molecular Geometry and Cu Coordination in Bicentric Copper Complexes. *Nat. Commun.* **2022**, *13* (1), 5122.
(29) Feng, J.; Zhang, L.; Liu, S.; Xu, L.; Ma, X.; Tan, X.; Wu, L.; Qian, Q.; Wu, T.; Zhang, J.; et al. Modulating Adsorbed Hydrogen Drives Electrochemical CO_2-to-C_2 Products. *Nat. Commun.* **2023**, *14* (1), 4615.
(30) Qiu, X.-F.; Huang, J.-R.; Yu, C.; Zhao, Z.-H.; Zhu, H.-L.; Ke, Z.; Liao, P.-Q.; Chen, X.-M. A Stable and Conductive Covalent Organic Framework with Isolated Active Sites for Highly Selective Electroreduction of Carbon Dioxide to Acetate. *Angew. Chem., Int. Ed.* **2022**, *61* (36), No. e202206470.
(31) Wu, Z.-Z.; Zhang, X.-L.; Yang, P.-P.; Niu, Z.-Z.; Gao, F.-Y.; Zhang, Y.-C.; Chi, L.-P.; Sun, S.-P.; DuanMu, J.-W.; Lu, P.-G.; Li, Y.-C.; Gao, M.-R. Gerhardtite as a Precursor to an Efficient CO-to-Acetate Electroreduction Catalyst. *J. Am. Chem. Soc.* **2023**, *145* (44), 24338−24348.
(32) Huang, L.; Liu, Z.; Gao, G.; Chen, C.; Xue, Y.; Zhao, J.; Lei, Q.; Jin, M.; Zhu, C.; Han, Y.; Francisco, J. S.; Lu, X. Enhanced CO_2 Electroreduction Selectivity toward Ethylene on Pyrazolate-Stabilized Asymmetric Ni−Cu Hybrid Sites. *J. Am. Chem. Soc.* **2023**, *145* (48), 26444−26451.
(33) Yang, X.; Li, X.; Huang, Y. Single-Atom Catalysis: A Promising Avenue for Precisely Controlling Reaction Pathways. *Front. Chem. Sci. Eng.* **2024**, *18* (7), 79.
(34) Gong, Y.-N.; Mei, J.-H.; Shi, W.-J.; Liu, J.-W.; Zhong, D.-C.; Lu, T.-B. Boosting CO_2 Photoreduction to Formate or CO with High Selectivity over a Covalent Organic Framework Covalently Anchored on Graphene Oxide. *Angew. Chem., Int. Ed.* **2024**, *63*, No. e202318735.
(35) Lu, M.; Zhang, M.; Liu, C.; Liu, J.; Shang, L.; Wang, M.; Chang, J.; Li, S.; Lan, Y. Stable Dioxin-Linked Metallophthalocyanine Covalent Organic Frameworks (COFs) as Photo-Coupled Electrocatalysts for CO_2 Reduction. *Angew. Chem., Int. Ed.* **2021**, *60* (9), 4864−4871.
(36) Yu, J.; Wang, Y.; Li, Y. A Two-Dimensional Covalent Organic Framework with Single-Atom Manganese for Electrochemical NO Reduction: A Computational Study. *Phys. Chem. Chem. Phys.* **2024**, *26* (21), 15120−15124.
(37) Rong, Y.; Liu, T.; Sang, J.; Li, R.; Wei, P.; Li, H.; Dong, A.; Che, L.; Fu, Q.; Gao, D.; et al. Directing the Selectivity of CO Electrolysis to Acetate by Constructing Metal-Organic Interfaces. *Angew. Chem., Int. Ed.* **2023**, *62* (45), No. e202309893.
(38) Liu, M.; Yang, S.; Fu, Y.; Yang, X.; Li, X.; He, J.; Xu, Q.; Zeng, G. Ladder Type Covalent Organic Frameworks Constructed with Natural Units for the Oxygen and Carbon Dioxide Reduction Reactions. *Chem. Eng. J.* **2024**, *488*, 150812.
(39) Guo, H.; Si, D.-H.; Zhu, H.-J.; Chen, Z.-A.; Cao, R.; Huang, Y.-B. Boosting CO_2 Electroreduction over a Covalent Organic Framework in the Presence of Oxygen. *Angew. Chem., Int. Ed.* **2024**, *63* (14), No. e202319472.
(40) Zhang, Y.; Cao, L.; Bai, G.; Lan, X. Engineering Single Cu Sites into Covalent Organic Framework for Selective Photocatalytic CO_2 Reduction. *Small* **2023**, *19* (22), 2300035.
(41) Lin, W.; Lin, F.; Lin, J.; Xiao, Z.; Yuan, D.; Wang, Y. Efficient Photocatalytic CO_2 Reduction in Ellagic Acid−Based Covalent Organic Frameworks. *J. Am. Chem. Soc.* **2024**, *146* (23), 16229−16236.
(42) Li, J.; Chen, Y.; Yao, B.; Yang, W.; Cui, X.; Liu, H.; Dai, S.; Xi, S.; Sun, Z.; Chen, W.; Qin, Y.; Wang, J.; He, Q.; Ling, C.; Wang, D.; Zhang, Z. Cascade Dual Sites Modulate Local CO Coverage and Hydrogen-Binding Strength to Boost CO_2 Electroreduction to Ethylene. *J. Am. Chem. Soc.* **2024**, *146* (8), 5693−5701.
(43) Singh, A.; Barman, S.; Rahimi, F. A.; Dey, A.; Jena, R.; Kumar, R.; Mathew, N.; Bhattacharyya, D.; Maji, T. K. Atomically Dispersed Co^{2+} in a Redox-Active COF for Electrochemical CO_2 Reduction to Ethanol: Unravelling Mechanistic Insight through *Operando* Studies. *Energy Environ. Sci.* **2024**, *17* (6), 2315−2325.
(44) Raciti, D.; Cao, L.; Livi, K. J. T.; Rottmann, P. F.; Tang, X.; Li, C.; Hicks, Z.; Bowen, K. H.; Hemker, K. J.; Mueller, T.; Wang, C. Low-Overpotential Electroreduction of Carbon Monoxide Using Copper Nanowires. *ACS Catal.* **2017**, *7* (7), 4467−4472.
(45) Jouny, M.; Luc, W.; Jiao, F. High-Rate Electroreduction of Carbon Monoxide to Multi-Carbon Products. *Nat. Catal.* **2018**, *1* (10), 748−755.
(46) Zhang, X.; Lou, Z.; Chen, J.; Liu, Y.; Wu, X.; Zhao, J.; Yuan, H.; Zhu, M.; Dai, S.; Wang, H.; et al. Direct OC-CHO Coupling towards Highly C_{2+} Products Selective Electroreduction over Stable Cu^0/Cu^{2+} Interface. *Nat. Commun.* **2023**, *14* (1), 7681.
(47) Yang, P.-P.; Zhang, X.-L.; Liu, P.; Kelly, D. J.; Niu, Z.-Z.; Kong, Y.; Shi, L.; Zheng, Y.-R.; Fan, M.-H.; Wang, H.-J.; Gao, M.-R. Highly Enhanced Chloride Adsorption Mediates Efficient Neutral CO_2 Electroreduction over a Dual-Phase Copper Catalyst. *J. Am. Chem. Soc.* **2023**, *145* (15), 8714−8725.
(48) Chang, X.; Li, J.; Xiong, H.; Zhang, H.; Xu, Y.; Xiao, H.; Lu, Q.; Xu, B. C−C Coupling Is Unlikely to Be the Rate-Determining Step in the Formation of C_{2+} Products in the Copper-Catalyzed Electrochemical Reduction of CO. *Angew. Chem., Int. Ed.* **2022**, *61* (2), No. e202111167.
(49) Li, H.; Wei, P.; Liu, T.; Li, M.; Wang, C.; Li, R.; Ye, J.; Zhou, Z.-Y.; Sun, S.-G.; Fu, Q.; et al. CO Electrolysis to Multicarbon Products over Grain Boundary-Rich Cu Nanoparticles in Membrane Electrode Assembly Electrolyzers. *Nat. Commun.* **2024**, *15* (1), 4603.
(50) Zhang, L.; Feng, J.; Wang, R.; Wu, L.; Song, X.; Jin, X.; Tan, X.; Jia, S.; Ma, X.; Jing, L.; Zhu, Q.; Kang, X.; Zhang, J.; Sun, X.; Han, B. Switching CO-to-Acetate Electroreduction on Cu Atomic Ensembles. *J. Am. Chem. Soc.* **2025**, *147* (1), 713−724.
(51) Shirzadi, E.; Jin, Q.; Zeraati, A. S.; Dorakhan, R.; Goncalves, T. J.; Abed, J.; Lee, B.-H.; Rasouli, A. S.; Wicks, J.; Zhang, J.; et al. Ligand-Modified Nanoparticle Surfaces Influence CO Electroreduction Selectivity. *Nat. Commun.* **2024**, *15* (1), 2995.
(52) Xie, G.; Guo, W.; Fang, Z.; Duan, Z.; Lang, X.; Liu, D.; Mei, G.; Zhai, Y.; Sun, X.; Lu, X. Dual-Metal Sites Drive Tandem Electrocatalytic CO_2 to C_{2+} Products. *Angew. Chem., Int. Ed.* **2024**, *63* (47), No. e202412568.
(53) Li, M.; Ma, Y.; Chen, J.; Lawrence, R.; Luo, W.; Sacchi, M.; Jiang, W.; Yang, J. Residual Chlorine Induced Cationic Active Species on a Porous Copper Electrocatalyst for Highly Stable Electrochemical CO_2 Reduction to C_{2+}. *Angew. Chem., Int. Ed.* **2021**, *60* (20), 11487−11493.
(54) Zhang, J.; Wang, Y.; Li, Y. Not One, Not Two, But at Least Three: Activity Origin of Copper Single-Atom Catalysts toward CO_2/

CO Electroreduction to C_{2+} Products. *J. Am. Chem. Soc.* **2024**, *146* (22), 14954−14958.
(55) Wang, X.; Ou, P.; Wicks, J.; Xie, Y.; Wang, Y.; Li, J.; Tam, J.; Ren, D.; Howe, J. Y.; Wang, Z.; et al. Gold-in-Copper at Low *CO Coverage Enables Efficient Electromethanation of CO_2. *Nat. Commun.* **2021**, *12* (1), 3387.

https://doi.org/10.1021/jacs.5c06660
J. Am. Chem. Soc. 2025, 147, 22132−22140